CrystEngComm

Accepted Manuscript

Diverse polyoxometalates-based metal–organic complexes constructed by a tetrazole- and pyridyl-containing asymmetric amide ligand or its *in-situ* transformed ligand†

Xiu-Li Wang*, Xing Rong, Dan-Na Liu, Hong-Yan Lin, Guo-Cheng Liu, Xiang Wang, Ge Song

Received (in XXX, XXX) Xth XXXXXXXXX 20XX, Accepted Xth XXXXXXXXX 20XX
DOI: 10.1039/b000000x

By introducing a tetrazole- and pyridyl-containing asymmetric amide ligand into polyoxometalates (POMs) systems, four POM-based complexes, namely, $H_4[Cu_2(TAAP)_4(H_2O)](Mo_8O_{26})_2\cdot 20H_2O$ (**1**), $H_2[Co(TAAP)_2(H_2O)_2](Mo_8O_{26})\cdot 11H_2O$ (**2**), $H_2[Ag_4(TAAP)_4(H_2O)_2(PMo_{12}O_{40})_2]\cdot 4H_2O$ (**3**), $H_4[Ag_2(AAP)_4(PW_{12}O_{40})_2]\cdot 2AAP\cdot 12H_2O$ (**4**) (TAAP = 3-(1H-Tetrazole-1-acetic acid amido) pyridine; AAP = 3-(acetic acid amido) pyridine) have been prepared under solvothermal (methanol-water mixed solvent) or hydrothermal conditions and structurally characterized. Compounds **1** and **2** are isostructural 3D structures, which are based on 3D $[M(TAAP)_2]_n^{2n+}$ metal-organic frameworks and noncoordinated $[Mo_8O_{26}]^{4-}$ polyanions templates. Compound **3** exhibits a dimeric structure constructed from two Keggin $[PMo_{12}O_{40}]^{3-}$ anions and a tetranuclear $[Ag_4(TAAP)_4(H_2O)_2]^{4+}$ subunit. Compound **4** is 2D supramolecular network based on 1D infinite chains, which are constructed by $[PW_{12}O_{40}]^{3-}$ and Ag-AAP subunit. In compound **4**, the AAP ligand was *in-situ* transformed from TAAP. The structural diversities show that POMs play key roles in the construction of final architectures and the *in-situ* transformation of TAAP. The title compounds represent the first examples of introducing tetrazole- and pyridyl-containing asymmetric amide ligand into the POMs system. The electrochemistry, photocatalysis and photoluminescence properties of the title compounds have been reported.

Introduction

Polyoxometalates (POMs), viewed as excellent inorganic ligands or noncoordinated templates due to their abundant O atoms, have been widely used to construct metal−organic complexes (MOCs) materials with various structures and properties.[1] The octamolybdate- and Keggin-based MOCs are two important branches, in which the Keggin anions usually acted as both inorganic ligands and noncoordinated templates, while the octamolybdate was often used as ligands.[2] The reports on octamolybdate as noncoordinated templates are relatively limited.[3]

From the synthetic point of view, the designing or selecting proper organic ligands with specific length, geometry, coordination sites and coordination ability is crucial to achieve the desired structures.[4] Up to now, a large amount of N-donor ligands, O-donor ligands and N/O-donor ligands have been widely used to construst POMs-based MOCs due to their abundant coordination sites and excellent coordination ability.[5] The N/O-donor ligands mainly include N-containing carboxylic acids, amide ligands and so on[6]. Some symmetric amide ligands such as 1,4-bis(3-pyridinecarboxamido)benzene, N,N'-bis(3-pyridinecarboxamide)-1,2-ethane, N,N'-bis(isonicotinoyl)-trans-1,2-diaminocyclohexane) etc have been reported.[7] However, the research on POMs-based MOCs based on asymmetric amide ligands are still limited.[8]

In this work, a tetrazole- and pyridyl-containing asymmetric amide ligand, namely, 3-(1H-Tetrazole-1-acetic acid amido) pyridine (TAAP) was employed to assemble with transition metal ions and POMs under hydrothermal or solvothermal conditions. The TAAP ligand has some remarkable features as follows: (i) Both the tetrazole and pyridyl rings may act as excellent coordination sites to coordinate with metal ions generating diverse structures; (ii) the amide groups with both the N–H hydrogen donor and C=O hydrogen acceptor may conduce to the formation of hydrogen bonds and supramolecular structures; (iii) the flexible nature of $–CH_2–$allows the ligands to bend freely to satisfy the coordination requirement of metal centers. To the best of our knowledge, research on the introduction of TAAP ligand into POMs systems has not been reported up to now (**Scheme 1**).

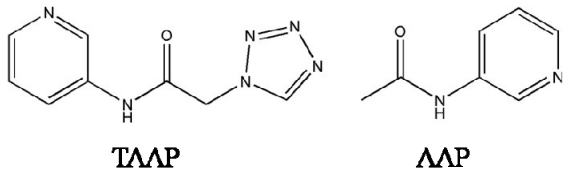

Scheme 1. The TAAP ligand and in-situ transformed AAP ligand from TAAP in this paper.

In the synthesis process of MOCs, some organic ligands may *in-situ* transform to other one or two new ligands.[9] Up to now, the examples of *in-situ* ligand transformation are relatively rare in POM-based MOCs.[10] In this work, by introducing a tetrazole- and

Department of Chemistry, Bohai University, Jinzhou, 121000, P. R. China. Fax: +86-416-3400158; Tel: +86-416-3400158; Email: wangxiuli@bhu.edu.cn

†Electronic Supplementary Information (ESI) available: IR Spectra, TG, and additional figures. CCDC 1456563-1456566. For ESI and crystallographic data in CIF or other electronic format see DOI: 10.1039/b000000x

pyridyl-containing asymmetric amide ligand into POMs systems, four POM-based complexes : $H_4[Cu_2(TAAP)_4(H_2O)](Mo_8O_{26})_2\cdot 20H_2O$ (**1**), $H_2[Co(TAAP)_2(H_2O)_2](Mo_8O_{26})\cdot 11H_2O$ (**2**), $H_2[Ag_4(TAAP)_4(H_2O)_2(PMo_{12}O_{40})_2]\cdot 4H_2O$ (**3**), $H_4[Ag_2(AAP)_4(PW_{12}O_{40})_2]\cdot 2AAP\cdot 12H_2O$ (**4**) (AAP=3-(acetic acid amido) pyridine) have been successfully synthesized under solvothermal (methanol-water mixed solvent) or hydrothermal conditions. In compound **4**, the AAP ligand was in-situ transformed from TAAP. The influence of the metal ions and POMs on the structures was discussed. The electrochemical behaviors of compounds **1**, **3** and **4** and photocatalysis properties of the title compounds were investigated. Moreover, the luminescent emissions of compounds **3** and **4** were studied at room temperature.

Experimental

All reagents and solvents for syntheses were purchased from commercial sources and used as received without further purification. The tetrazole- and pyridyl-containing asymmetric amide ligand TAAP was prepared according to the reported procedure.[11] Powder X-ray diffraction (PXRD) patterns were recorded on an Ultima IV with D/teX Ultra diffractometer at 40 kV, 40 mA with Cu Kα (λ = 1.5406 Å) radiation in the 2θ range of 5-50°. FT-IR spectra (KBr pellets) were taken on a Magna FT-IR 560 Spectrometer. Thermogravimetric analyses (TGA) were performed on a SDT 2960 Simultaneous DSC-TGA instrument under flowing N_2 atmosphere with a heating rate of 10 °C·min^{-1}. A CHI 440 Electrochemical Quartz Crystal Microbalance was used for the electrochemical experiments. A conventional three-electrode cell was used at room temperature. The title compounds bulk-modified carbon-paste electrodes (CPEs) were used as the working electrodes. An SCE and a platinum wire were used as reference and auxiliary electrodes, respectively. UV-Vis absorption spectra were obtained using a SP-1901 UV-Vis spectrophotometer.

X-Ray crystallography

Crystallographic data for compounds **1**–**4** were collected on a Bruker Smart Apex II diffractometer with Mo Kα radiation (λ = 0.71069 Å) by ω and θ scan mode at 293 K. All the structures were solved by direct methods and refined on F^2 by full-matrix least squares using the SHELXL package.[12] For these compounds, all hydrogen atoms attached to water molecules were not located, but were included in the structure factor calculations. In compounds **1** and **2**, the unit cell includes a large region of disordered solvent molecules, which could not be modeled as discrete atomic sites. Thus, the SQUEEZE routine of PLATON was applied to remove the contributions to the scattering from the solvent molecules. The reported refinements are of the guest-free structures using the *.hkp files produced by using the SQUEEZE routine.[13] The amount of water molecules of compounds **1** and **2** came from the TG experiment. During the refinement, the command 'isor' was used to restrain the atoms O34 of compound **1** and C30 of compound **4**. The detailed crystal data and stuctures refinement for **1**–**4** are given in **Table 1**. Selected bond lengths and angles are listed in **Table S1**†. Crystallographic data for the structures reported in this paper have been deposited in the

Table 1 Crystallographic data for compounds **1**−**4**

Compound	**1**	**2**	**3**	**4**
Empirical formula	$C_{32}H_{78}Cu_2Mo_{16}N_{24}O_{77}$	$C_{16}H_{44}CoMo_8N_{12}O_{41}$	$C_{32}H_{46}Ag_4Mo_{24}N_{24}O_{90}P_2$	$C_{42}H_{76}Ag_2N_{12}O_{98}P_2W_{24}$
Formula weight	3693.28	1887.08	5002.91	7007.23
Crystal system	Orthorhombic	Orthorhombic	monoclinic	Triclinic
Space group	*Cmca*	*Cmca*	*P2(1)/n*	*P -1*
a (Å)	26.9829(10)	27.0900(13)	12.9320(4)	12.7322(10)
b (Å)	37.6059(15)	38.2760(13)	18.9820(6)	13.6706(11)
c (Å)	19.3314(7)	19.1070(8)	21.4570(7)	16.5220(14)
α (°)	90	90	90	89.582(2)
β (°)	90	90	102.7290(10)	87.082(2)
γ (°)	90	90	90	86.877(2)
V (Å^3)	19615.9(13)	19812.0(14)	5137.7(3)	2867.7(4)
Z	8	16	2	1
D_c (g cm^{-3})	2.257	2.265	3.234	4.057
μ (mm^{-1})	2.491	2.376	3.724	24.434
F (000)	12672	12880	4704	3096
Reflection collected	69989	71350	29140	16447
Unique reflections	12443	12511	9051	10111
parameters	613	628	793	811
R_{int}	0.0441	0.0514	0.0195	0.0676
GOF	1.081	1.083	1.031	1.029
R_1^a [$I > 2\sigma(I)$]	0.0561	0.0475	0.0486	0.0722
wR_2^b (all data)	0.1745	0.1507	0.1121	0.2218

$^a R_1 = \sum \| F_o | - | F_c \| / \sum | F_o |$. $^b wR_2 = \{\sum[w(F_o^2 - F_c^2)^2]/\sum[w(F_o^2)^2]\}^{1/2}$

Cambridge Crystallographic Data Center with CCDC Numbers 1456563–1456566.

Preparation of compounds 1−4

Synthesis of $H_4[Cu_2(TAAP)_4(H_2O)_2](Mo_8O_{26})_2\cdot 20H_2O$ (1). A mixture of $CuCl_2\cdot 2H_2O$ (0.085 g, 0.5 mmol), TAAP (0.020 g, 0.1 mmol), $(NH_4)_6Mo_7O_{24}\cdot 4H_2O$ (0.124 g, 0.1 mmol), H_2O (5 mL) and methanol (5 mL) was added in a 12 mL glass vial and heated at 85°C for 4 days. After slow cooling to room temperature, green block crystals of **1** were filtered (final pH = 2.8) and washed off the white precipitate with distilled water, and dried at room temperature in a desiccator, giving a yield of 34% based on Mo. Anal. Calcd for $C_{32}H_{78}Cu_2Mo_{16}N_{24}O_{77}$: C 10.41; H, 2.13; N, 9.10%. Found: C, 10.38; H, 2.09; N, 9.15%. IR (KBr pellet, cm^{-1}): 3502(s), 3081(w), 2360(s), 1869(w), 1716(w), 1687(s), 1552(s), 1490(m), 1110(m), 948(s), 910(s), 881 (s), 665(s).

Synthesis of $H_2[Co(TAAP)_2(H_2O)_2](Mo_8O_{26})\cdot 11H_2O$ (2). The compound **2** was prepared in the same way as compound **1** except that $Co(NO_3)_2\cdot 6H_2O$ (0.146 g, 0.5 mmol) was used instead of $CuCl_2\cdot 2H_2O$. Pink block crystals of **2** were obtained and washed off the purple precipitate with distilled water to give a yield of 32% (final pH = 3.4). Anal. Calcd for $C_{16}H_{44}CoMo_8N_{12}O_{41}$: C 10.18; H, 2.35; N, 8.91%. Found: C, 10.15; H, 2.42; N, 8.89%. IR (KBr pellet, cm^{-1}): 3502(m), 3198(m), 3070(w), 2362(m), 1709(m), 1622(s), 1558(s), 1490(m), 1417(m), 1105(m), 941(s), 906(m), 849(m), 659(m).

Synthesis of $H_2[Ag_4(TAAP)_4(H_2O)_2(PMo_{12}O_{40})_2]\cdot 4H_2O$ (3). A mixture of $AgNO_3$ (0.150 g, 0.883 mmol), TAAP (0.020 g, 0.1 mmol), $H_3PMo_{12}O_{40}\cdot 13H_2O$ (0.300 g, 0.145 mmol), NH_4VO_3 (0.036 g, 0.307 mmol) and H_2O (10 mL) was stirred for 30 min at the room temperature. The pH value was then adjusted to about 2 using 1.0 M $NH_3\cdot H_2O$. The suspension was transferred to a Teflon lined autoclave (25 mL) and kept at 120 °C for 4 days. After slowly cooled to room temperature, orange block crystals of **3** were filtered off (final pH = 1.8) the yellow precipitate and washed with distilled water, dried in a desiccator at room temperature to give a yield of 25% based on Mo. Anal. Calcd for $C_{32}H_{46}Ag_4Mo_{24}N_{24}O_{90}P_2$: C 7.68; H, 0.93; N, 6.72%. Found: C, 7.62; H, 0.99; N, 6.77%. IR (KBr pellet, cm^{-1}): 3471 (s), 3081 (w), 2370 (m), 1690(w), 1654 (m), 1561 (m), 1054 (s), 958 (s), 885 (m), 806 (s), 669 (m).

Synthesis of $H_4[Ag_2(AAP)_4(PW_{12}O_{40})_2]\cdot 2AAP\cdot 12H_2O$ (4). Compound **4** was prepared in the same way as **3** except that $H_3PW_{12}O_{40}$ (0.300 g, 0.104 mmol) was used instead of $H_3PMo_{12}O_{40}\cdot 13H_2O$. Red block crystals of **4** were obtained (final pH = 1.7) and filtered off the yellow precipitate, then washed with distilled water. Yield 28% based on W. Anal. Calcd for $C_{42}H_{76}Ag_2N_{12}O_{98}P_2W_{24}$: C 7.20; H, 1.09; N, 2.40%. Found: C, 7.18; H, 1.06; N, 2.43%. IR (KBr pellet, cm^{-1}): 3570(w), 3115 (m), 2356 (m), 1646 (m), 1545 (s), 1442(w), 1274 (m), 1058 (s), 956 (s), 882 (m), 798 (s).

Preparation of compounds 1，3 and 4 bulk-modified CPEs: The compound **1** bulk-modified CPE (**1**–CPE) was fabricated by mixing 0.10 g graphite powder and 0.010 g compound **1** in an agate mortar for approximately 60 min to get a uniform mixture; then 0.16 mL paraffin oil was added and stirred with a glass rod. The homogenized mixture was packed into a 3 mm inner diameter glass tube and the tube surface was wiped with weighing paper. The electrical contact was established with the copper wire. In a similar manner, **3**–CPE and **4**–CPE were made with compounds **3** and **4**，respectively.

Results and discussion

Structural description

$H_4[Cu_2(TAAP)_4(H_2O)](Mo_8O_{26})_2\cdot 20H_2O$ (1) and **$H_2[Co(TAAP)_2(H_2O)_2](Mo_8O_{26})\cdot 11H_2O$ (2)** Single-crystal X-ray diffraction analyses show that compounds **1** and **2** are isostructural (**Fig. 1a** and **Fig. S1†**). As a result, compound **1** is discussed in detail as the representative example. The compound **1** consists of two Cu^{II} ions, two $Mo_8O_{26}^{4-}$ anions, four TAAP ligands, one coordinated water molecule and twenty lattice water

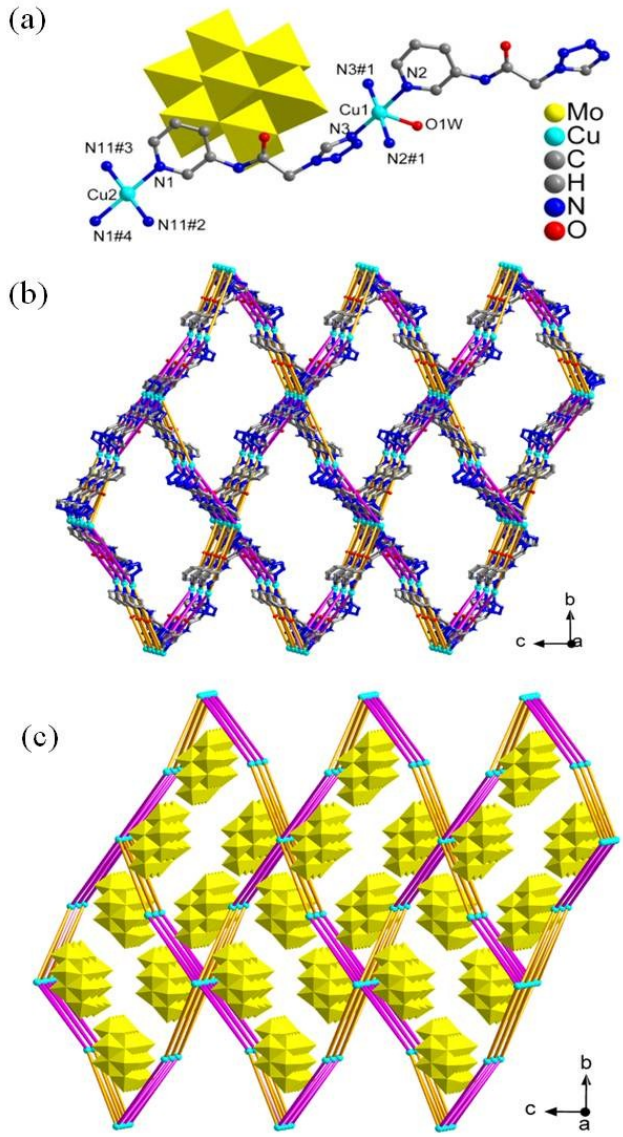

Fig. 1 (a) The coordination environment of the Cu^{II} ions in **1**. All H atoms and lattice water molecules are omitted for clarity. Symmetry code: #1 –x +1, y, z; #2 x–1/2, –y+1, z–1/2; #3 –x+1, y–1/2, –z+3/2; #4 –x+1/2, –y+1/2, –z+1; (b) The 3D framework constructed by TAAP and Cu^{II} ions;

(c) The $Mo_8O_{26}^{4-}$ templates reside in the 3D framework of **1**.

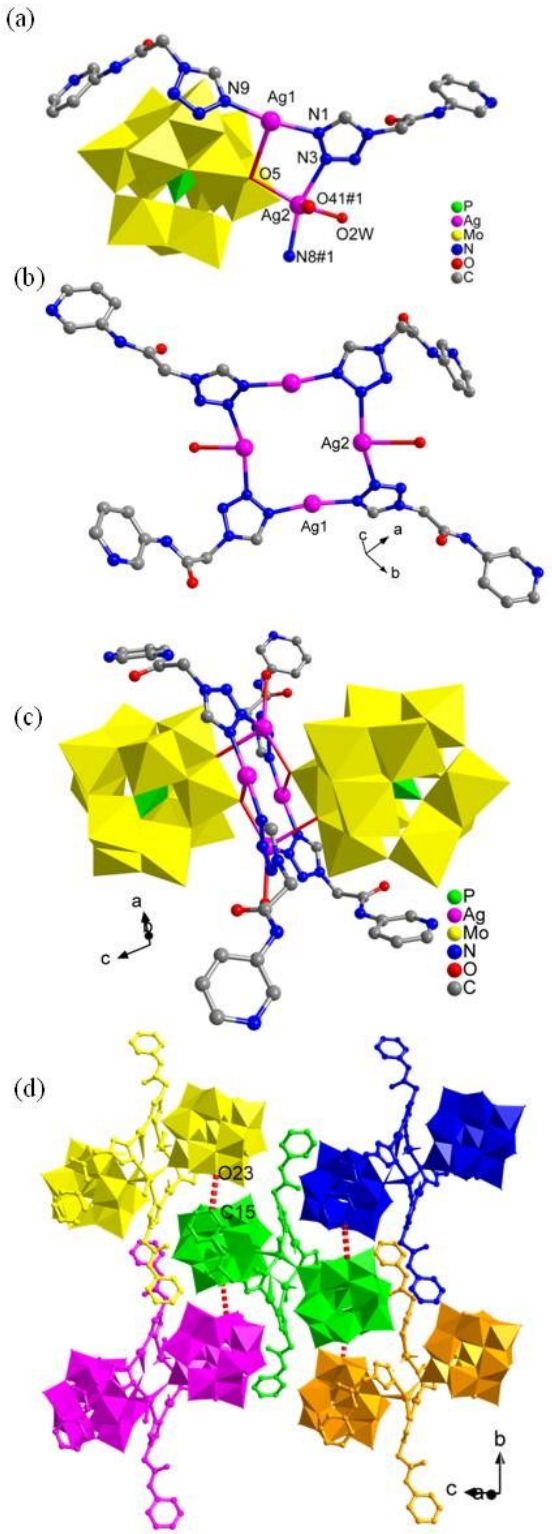

Fig. 2 (a) The coordination environment of the Ag^I ions in **3**. All H atoms and lattice water molecules are omitted for clarity. Symmetry code: #1 – x, -y-1, -z; (b) View of the tetranuclear $[Ag_4(TAAP)_4(H_2O)_2]^{4+}$ subunit in **3;** (c) Dimeric structure of **3**. All H atoms and lattice water molecules are omitted for clarity. (d) The 2D supramolecular structure formed *via* hydrogen bonds in **3**.

molecules. In order to balance the charges, four protons were added to the molecular formula. There are two crystallographically independent Cu^{II} ions in **1**. The Cu1 ion is five-coordinated, defined by four N atoms from two tetrazole and two pyridyl rings of four TAAP ligands and one O atom from a water molecule. The bond distances around Cu1 ion are 2.036(6) and 2.037(6) Å for Cu–N, 2.341(7) Å for Cu–O and the bond angles are 87.3(3) –176.6(2)° for N–Cu–N. Different from Cu1, Cu2 is coordinated by four N atoms from two tetrazole and two pyridyl rings of four independent TAAP ligands. The bond distances around Cu2 ion are 2.024(6) and 2.053(6) Å for Cu–N, and the bond angles are 88.1(2) –179.998(1)° for N–Cu–N. Due to the flexible nature of the TAAP ligand, two types of TAAP ligands with different dihedral angles appeared. The dihedral angles of the two types of TAAP ligands between pyridyl rings and tetrazole rings are 33.86º (plane 1: N2 C9 C10 C11 C12 C16; plane 2: C14 N9 N10 N11 N12) and 61.36º (plane 1: C8 N3 N5 N6 N7; plane 2: N1 C1 C2 C3 C4 C5), respectively. The adjacent Cu^{II} ions are connected by TAAP ligands to form a 3D metal-organic framework (**Fig. 1b**). The $Mo_8O_{26}^{4-}$ anions are serving as templates in the 3D frameworks (**Fig. 1c**).

In our previous work，we have obtained three octamolybdate-based MOCs with pyridyl-carboxylate amide ligand.[6] In those compounds, octamolybdate acting as inorganic building blocks formed 1D or 2D structures. When the tetrazole- and pyridyl-containing amide ligand was used, we obtained two 3D frameworks with octamolybdate acting as templates. The results illustrated that the tetrazole- and pyridyl-containing amide ligand may be more helpful to form the higher dimensional complexes.

To further investigate the effect of metal ions on the structural diversities of the TAAP-Mo_8O_{26}-based complexes and search for new isomers in TAAP-Mo_8O_{26} system, we tried to employ different metal ions such as Ag^I. Unfortunately, we could not acquire the crystals of Ag^I-TAAP-Mo_8O_{26} in the similar conditions, even other reaction temperature. Based on these, could the Ag^I compounds be obtained in other POMs system?

$H_2[Ag_4(TAAP)_4(H_2O)_2(PMo_{12}O_{40})_2]\cdot 4H_2O$ (3).

When $AgNO_3$ was used in TAAP-$PMo_{12}O_{40}$ system, the compound **3** with absolutely different structure was obtained. The asymmetric unit of **3** contains two crystallographically independent Ag^I ions, two TAAP ligands, one $PMo_{12}O_{40}^{3-}$ (PMo_{12}) anion, one coordinated water molecule and two lattice water molecules. In order to balance the charges, two protons were added to the molecular formula. As shown in **Fig. 2a**, the Ag1 ion exhibits a three-coordinated mode with two N atoms from two tetrazole rings of two TAAP ligands and one terminal O atom of one PMo_{12} anion. The bond distances around Ag1 ion are 2.127(8) and 2.153(8) Å for Ag–N, 2.819(8) Å for Ag–O and the bond angles are 170.7(3)° for N–Ag–N. The Ag2 ion is five-coordinated by two N atoms from two tetrazole rings of two TAAP ligands, two O atoms of two PMo_{12} anions and one O atom of water molecule. The bond distances around Ag2 ion are 2.283(8) and 2.343(8) Å for Ag–N, 2.449(8)–2.643(8) Å for Ag–O and the bond angles are 157.3(3)° for N–Ag–N, 84.38(2)–147.08(3)° for O–Ag–O. In compound **3**, a tetranuclear $[Ag_4(TAAP)_4(H_2O)_2]^{4+}$ subunit (**Fig. 2b**) connected with two

Keggin PMo_{12} anions *via* Ag–O bond forming a dimeric structure (**Fig. 2c**). There are two types of TAAP ligands with different dihedral angles appeared in the dimeric structure. The dihedral angles of the two types of TAAP between pyridyl rings and tetrazole rings are 62.78º (plane 1: N12 C12 C13 C14 C15 C16; plane 2: C9 N7 N8 N9 N10) and 83.97º (plane 1: N6 C5 C6 C7 C8 C4; plane 2: C1 N1 N2 N3 N4).

Furthermore, the detailed structural analysis reveals that these dimers are further connected via hydrogen-bonding interactions (C(15)–H(15A)···O(23) = 3.100 Å) between the N atom from TAAP and oxygen atom from PMo_{12} anion, forming a 2D supramolecular architecture (**Fig. 2d**).

$H_4[Ag_2(AAP)_4(PW_{12}O_{40})_2]\cdot 2AAP\cdot 12H_2O$ (4).

When $H_3PW_{12}O_{40}$ instead of $H_3PMo_{12}O_{40}\cdot 13H_2O$ was used and the other experimental conditions unchanged as those for the synthesis of **3**, compound **4** with different structure was obtained. Single-crystal X-ray diffraction analysis shows that the asymmetric unit of **4** consists of one Ag^I ion, two coordinated AAP ligands, one PW_{12} anion, one free AAP molecule and six lattice water molecules. The ligand AAP was in-situ transformed by TAAP ligand in the synthesis process of compound **4**. In order to balance the charges, four protons were added to the molecular formula. As shown in **Fig. 3a**, the Ag^I ion is six-coordinated, defined by four O atoms from three PW_{12} anions and two N atoms from two pyridyl rings of two AAP ligands.The bond distances around Ag1 ion are 2.165(19) and 2.22(2) Å for Ag–N, 2.703(2)–2.876(2) Å for Ag–O and the bond angles are 142.8(7)° for N–Ag–N. 56.94(3)–142.55(7)° for O–Ag–O. If the ligands AAP were omitted, an infinited 1D inorganic chains could be observed (**Fig. 3b**). Two AAP ligands hang on two sides of Ag^I ions showing the integrated 1D chains (**Fig. S2**). A detailed structural analysis reveals the adjacent 1D chains were connected *via* hydrogen-bonding interactions (C(17)–H(17A)···O(3) = 3.169 Å) between the C atoms from AAP ligands and O atoms from PW_{12} anions forming a 2D supramolecular structure(**Fig. 3c**).

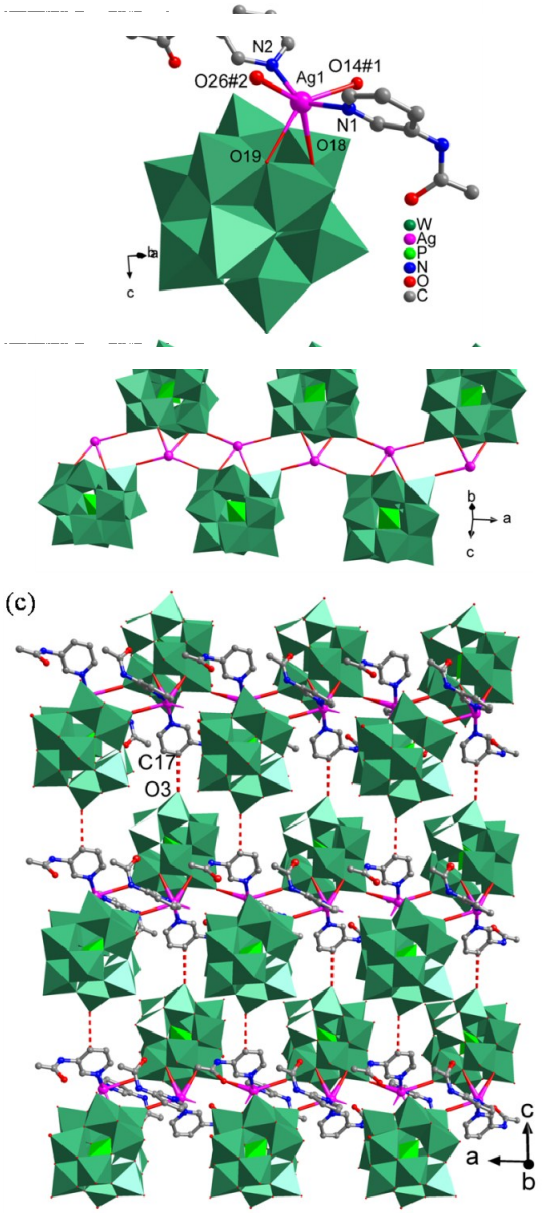

Fig. 3 (a) The coordination environment of the Ag^I ion in **4**. All H atoms and lattice water molecules are omitted for clarity. Symmetry code: #1 – x+1,–1–y,1–z. (b) The 1D inorganic chain in **4** (c) The 2D supramolecular structure via hydrogen-bonding interactions in **4**.

The *in-situ* tansformation of AAP

It is interesting that compound **4** and the *in situ* synthesis of APP are simultaneously generated under the hydrothermal reaction condition. The starting TAAP reagent was converted into APP ligand under the presence of the $PW_{12}O_{40}^{3-}$ polyanion, Ag^I ion and NH_4VO_3 in hydrothermal conditions (**Scheme 2**). The in-situ ligand reaction mechanism is complicated and elusive, as is reported by other groups.[14] Further insight into the nature of this reaction process, the APP ligand was generated from the single C–N bond cleavage of TAAP.[15] In the synthesis process of compound **3**, when other Keggin-type $H_3PMo_{12}O_{40}$ instead of $H_3PW_{12}O_{40}$ was used, the APP ligand could not be observed under the same hydrothermal condition. Thus, the $H_3PW_{12}O_{40}$ may play a crucial role in the process of *in-situ* transformation of TAAP. Besides, in the synthesis process of compounds **1** and **2**, the TAAP ligand also did not transform to AAP in solvothermal conditions, which further illustrated the importance of $H_3PW_{12}O_{40}$ in the *in-situ* ligand transformation process.

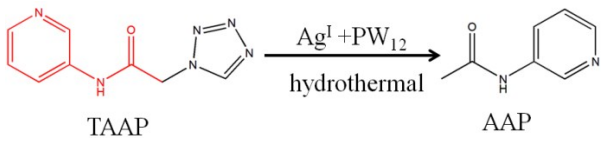

Scheme 2.The *in-situ* tansformation of AAP from TAAP.

The role of metal ions, solvents, temperature, POMs on the construction of the title compounds

In this work, we selected a tetrazole- and pyridyl-containing asymmetric amide as organic ligand, octamolybdate and two kinds of Keggin polyanions as inorganic building blocks to investigate their influence on the assembly and structures of the POM-based MOCs (**Scheme 3**).

As described above, compounds **1** and **2** are isostructural with the octamolybdate polyanions acting as templates, which indicate that the central Cu^{II} and Co^{II} ions have no obvious effect on the

final networks due to their same charges, similar sizes and similar properties. Compounds **1** and **2** are obtained in solvothermal

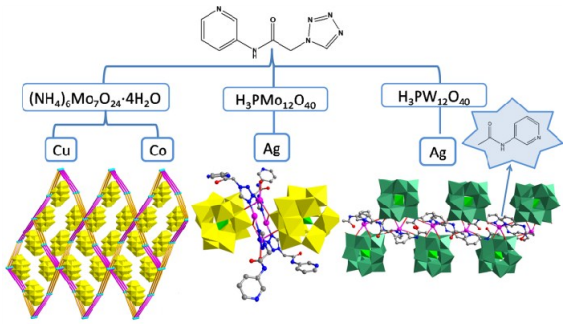

Scheme 3. Schematic illustration of influence of different POMs and metal ions on the structures of **1**–**4**.

conditions (methanol-water mixed solvent). We tried to synthesize these compounds under hydrothermal conditions. Unfortunately, no crystals could be obtained, which indicated the solvents have great effect on the formation of crystals. Otherwise, the different kinds of Keggin polyanions have significant effect on the architectures of compounds **3** and **4** in the same conditions. In compound **3**, two Keggin PMo_{12} anions acting as monodentate ligands coordinated to the Ag^{I} ions from a tetranuclear $[Ag_4(TAAP)_2(H_2O)_2]^{4+}$ subunit *via* Ag–O bond forming a dimeric structure. In compound **4**, the Keggin PW_{12} anions as four-connected inorganic ligands linked the $[Ag(APP)_2]^{+}$ subunits to form infinited 1D chains. It's worth noting that the TAAP liagnd *in-situ* transformed to AAP ligand in compound **4**. The results indicated that the difference of Keggin polyanions not only can influnce the final strucrures but also have great impact on the *in-situ* transformation of ligand in this system. We also tried to synthesize compounds **3** and **4** in other reaction temperatures. When the reaction temperature was 160 °C, the crystal yields are very low for compounds **3** and **4**. When the reaction was performed under 100 °C, only precipitates were obtained. Thus, the reaction temperatures is curical for the formation of crystals and 120 °C is the optimum temperature.

PXRD, IR spectra and TGA of compounds 1–4

The PXRD patterns for compounds **1**–**4** are presented in the Fig. S3. The diffraction peaks of the simulated and experimental patterns match well, thus indicating that **1**–**4** exhibit good phase purities. The IR spectra of compounds **1**–**4** are shown in Fig. S4. The characteristic bands at 947, 911, 887, 692 cm^{-1} for **1** and 940, 897, 851, 659 cm^{-1} for **2** are attributed to the ν(Mo=O), ν(Mo–O–Mo), respectively.[16] In the spectrum of **3**, the characteristic bands at 1058, 962, 885 and 800 cm^{-1} are attributed to ν(P-O), ν(Mo-O_d), and ν(Mo-$O_{b/c}$-Mo), respectively.[17] For **4**, the bands at 1054, 954, 879 and 788 cm^{-1} are the characteristic peaks of ν(P-O_a), ν(W-O_d) and ν(W-$O_{b/c}$-W), respectively.[18] The bands at 3078 cm^{-1} for **1**, 3071 cm^{-1} for **2**, 3081 cm^{-1} for **3** and 3097 cm^{-1} for **4** are due to the N–H stretching vibrations.[19] The characteristic bands observed at 1716, 1635 cm^{-1} for **1**, 1709, 1616 cm^{-1} for **2**, 1695, 1654 cm^{-1} for **3** and 1716, 1648 cm^{-1} for **4** can be ascribed to the strecthing and bending vibration of C=O.[20] The bands around 3400 cm^{-1} are associated with the water molecules. TGA of compounds **1**–**4** were performed from the room temperature to 800°C (Fig. S5). Compounds **1**–**4** have two distinct steps of weight losses, respectively. In the TG curves of compounds **1** and **2**, the first weight loss step corresponds to the loss of twenty-one lattice/coordinated water molecules 10.03% (calcd. 10.24%) for **1** and thirteen lattice/coordinated water molecules 12.79% (calcd. 12.41%) for **2**. The first weight losses of 2.42 % for **3** and 3.22 % for **4** are consistent with the removal of lattice/coordinated water molecules (calcd. 2.16% and 3.08%), respectively. Then, the second sharp weight losses for **1**–**4** are corresponding to the collapse of the frameworks and loss of the organic ligands.

Electrochemical property

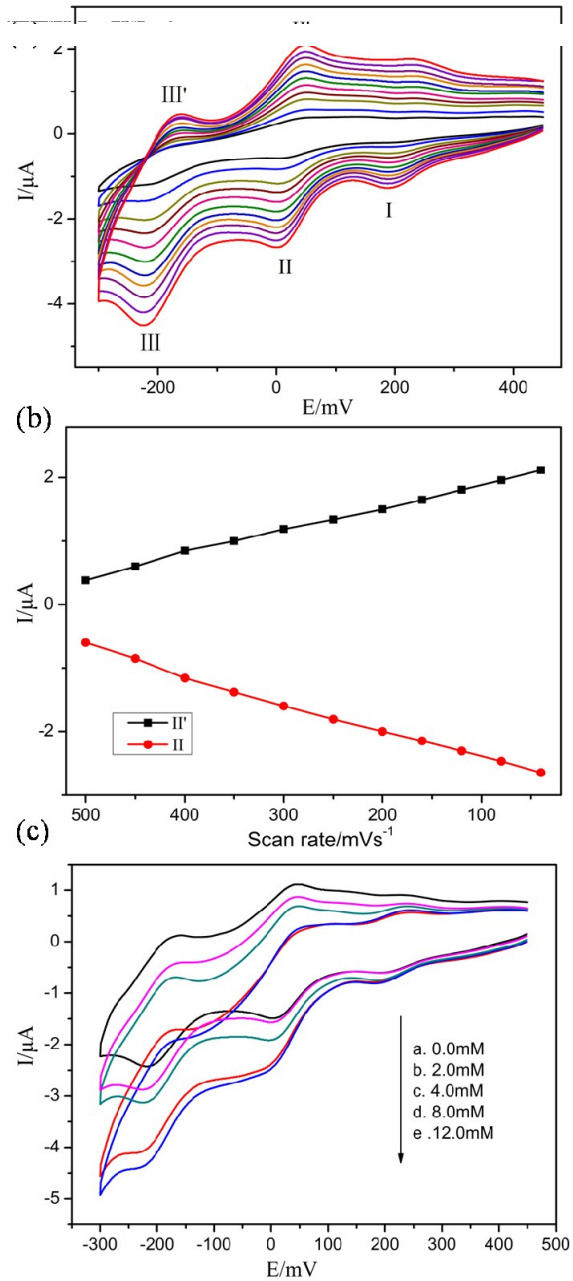

Fig. 4 (a) Cyclic voltammograms of the **1**–CPE in 0.1 M H_2SO_4 + 0.5 M Na_2SO_4 aqueous solution at different scan rates (from inner to outer: 40, 80, 120, 160, 200, 250, 300, 350, 400, 450, 500 mVs^{-1}); (b) The dependence of anodic peak (II) and cathodic peak (II') currents on scan

rates for **1**–CPE; (c) Cyclic voltammograms of **1**-CPE in 0.1 M H_2SO_4 + 0.5 M Na_2SO_4 solution containing 0.0–12.0 mM H_2O_2.

In order to investigate the electrochemical behaviors of these compounds, the title compounds bulk-modified CPEs were made. Because the electrochemical behaviors of compounds **1** and **2** are similar, so compound **1** has been taken as an example. The electrochemical behaviours of **1**–CPE, **3**–CPE and **4**–CPE in 0.1 M H_2SO_4 + 0.5 M Na_2SO_4 aqueous solution at different scan rates are presented. The **1**–CPE and **3**–CPE exhibit three pairs of redox peaks in the potential range of –300 to + 450 mV (**Fig. 4a**), –250 to 750 mV (**Fig. S6a**), respectively, and the **4**–CPE shows two pairs of redox peaks in the potential range of –900 to 100 mV (**Fig. S7a**), which can be attributed to the redox of Mo_8, PMo_{12} and PW_{12} polyanions, respectively.[21] The mean peak potentials $E_{1/2} = (E_{pa} + E_{pc})/2$ are +215 (I–I'), +25 (II–II') and –191 mV (III–III') (120 mVs^{-1}) for **1**–CPE, +396 (I–I'), +87 (II–II')and –120 mV (III–III') (120 mVs^{-1}) for **3**–CPE, and –530 (I–I') and –745 mV (II–II') (120 mVs^{-1}) for **4**–CPE, respectively. The peak potentials change gradually with the scan rates increasing: the cathodic peak potentials shift toward the negative direction and the corresponding anodic peak potentials to the positive direction. The peak currents are proportional to the scan rates up to 500 mVs^{-1}, indicating that the redox processes of the **1**–CPE, **3**–CPE and **4**–CPE are surface-controlled [22] (**Fig. 4b, Fig. S6b** and **Fig. S7b**). It is well known that POMs can electrocatalyze the reduction of some anions. In this paper, **1**–CPE, **3**–CPE and **4**–CPE show good electrocatalytic activities toward the reduction of hydrogen peroxide. As can be seen from **Fig. 4c, Fig. S6c** and **Fig. S7c**, for **1**–CPE, **3**–CPE and **4**–CPE, with the addition of hydrogen peroxide, all the reduction peak currents increase gradually and the corresponding oxidation peak currents decrease, suggesting that the reduction of hydrogen peroxide is mediated by the reduced species of Mo_8 in compound **1**, PMo_{12} in compound **3** and PW_{12} in compound **4**.[23]

Photocatalytic property

At present, the POMs-based MOCs have been proved good photocatalysts in degrading some organic substances under UV or visible light.[24] Herein, we selected an organic dye methylene blue (MB) as a model pollutant in aqueous media to investigate the photocatalytic performance of compounds **1**–**4** under UV irradiation from a 125 W Hg lamp, visible light irradiation from a 350 W Xe lamp equipped with a long-pass filter (400 nm cutoff) and sunlight irradiation. As shown in **Fig. 5** and **Fig. S8–S10** (top), the absorption peaks of MB decreased obviously with increasing reaction time for compounds **1**–**4** under UV irradiation. Moreover, the concentrations of MB (C) *versus* bushreaction time (t) for the title compounds were plotted. The degradation ratio of MB reaches 95.86 % for **1**, 92.22 % for **2**, 72.73 % for **3** and 92.27 % for **4** during 100 min. Additionally, PXRD patterns of the title compounds after the UV irradiation photocatalytic reactions have been recorded, which match with the simulated ones except for some intensity differences (**Fig. S3**). The results suggest that the title compounds possess good stability in the photodegradation of MB process. Due to the good stability and excellent photocatalytic performances under UV irradiation, we further performed photocatalytic tests of the title compounds towards the degradation of MB under visible light irradiation and sunlight irradiation, which can make the photocatalytic process more conducive to practical application. To the best of our knowledge, reports on the photocatalytic activity of POMs-based MOCs under visible light irradiation or sunlight irradiation are still very limited. As is shown in **Fig.5** and **Fig. S8–S10**, the absorption peaks of MB also decreased with increasing reaction time for compounds **1**–**4** under visible light and sunlight irradiation. The concentrations of MB (C) *versus* reaction time (t) for the title compounds were also plotted (**Fig.6**). The calculation results show that approximately 78.66 % for **1**, 63.40 % for **2**,

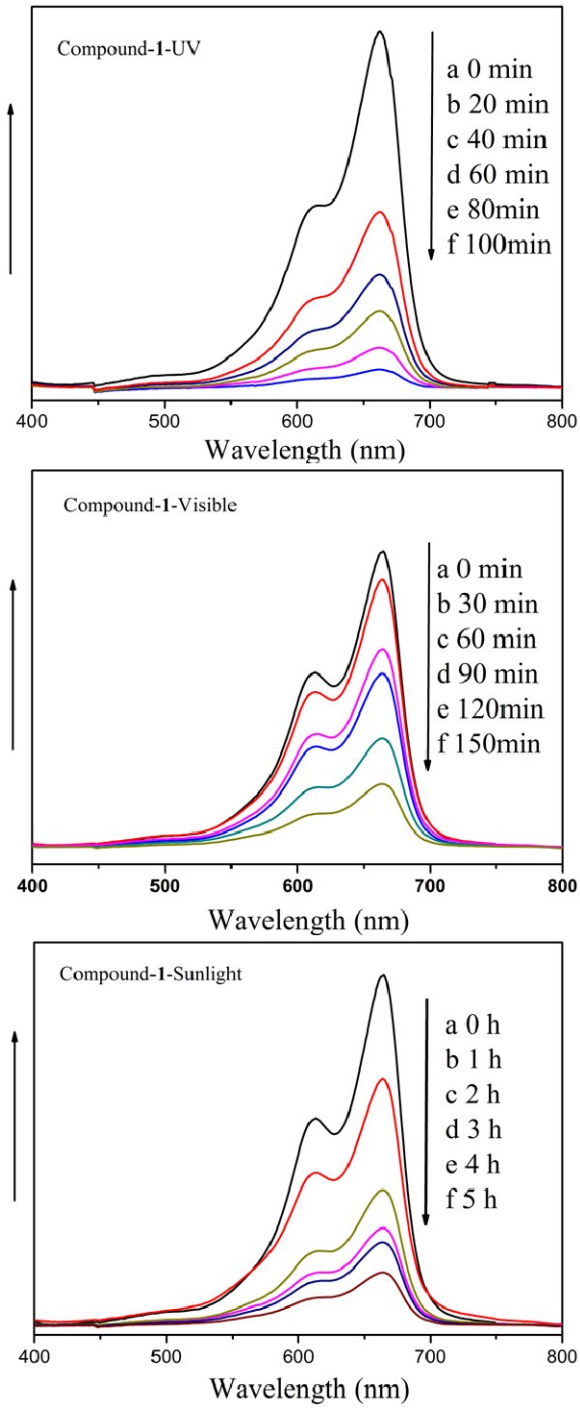

Fig.5 Absorption spectra of the MB solution during the decomposition

reaction under UV irradiation (top); visible light irradiation (middle) and sunlight irradiation (bottom) with the presence of compound **1**.

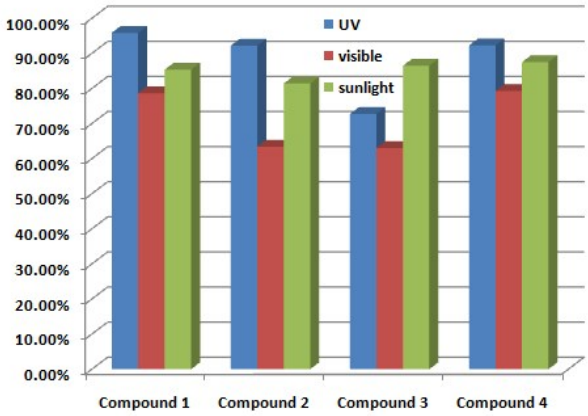

Fig.6 The degradation ratio of MB for compounds **1**–**4** under UV, visible light and sunlight irradiation.

63.03 % for **3** and 79.27 % for **4** of MB has been decomposed during 150 min under visible light irradiation and 85.36 % for 1, 81.43 % for 2, 86.48 % for 3 and 87.50 % for 4 of MB has been decomposed during 5 hours under sunlight irradiation.

Luminescent Properties.

Based on the excellent luminescent properties of coordination polymers with d^{10} metals,[25] the photoluminescent properties of compounds **3**-**4** have been investigated in the solid state at room temperature in this work. The emission peaks are shown in **Fig. S11**. The emission peaks of **3** and **4** are 450 nm (λ_{ex} = 320 nm) and 448 nm (λ_{ex} = 320 nm), respectively. To know the emission nature, the luminescent property of the free TAAP ligand was studied. The free TAAP ligand exhibits a strong emission peak at 412 nm upon excitation at 320 nm. Obviously, the emission peaks of **3** and **4** exhibit the distinct red shifts compared with the TAAP ligand, which may come from the ligand-to-metal charge-transfer transition (LMCT) involving the TAAP ligand and the central metal Ag^{I} ions.[26]

Conclusions

In conclusion, we have designed and synthesized four metal-organic complexes with various structures by introducing the tetrazole- and pyridyl-containing asymmetric amide ligand into POM systems. This work will suggest that suitable ligand is very important to obtain novel POMs-based MOCs and different Keggin POMs play crucial roles in the consruction of final structures and the *in-situ* transformation of ligand TAAP. The title compounds represent the first examples of introducing tetrazole- and pyridyl-containing asymmetric amide ligand into the POMs system. Compounds **1**, **3** and **4** exhibit good electrocatalytic behaviors toward the reduction of H_2O_2 and compounds **1**–**4** possess good photocatalytic activities for the degradation of MB under UV, visible light and sunlight irradiation. The luminescent properties of compounds **3** and **4** in the solid state at room temperature were also reported. Further work for preparing POM-based inorganic-organic compounds based on asymmetric amide ligands is in progress.

Acknowledgements

This work was fnancially supported by the National Natural Science Foundation of China (No. 21471021, 21401010 and 21501013) and Program for Distinguished Professor of Liaoning Province (No. 2015399).

Notes and references

1 (a) X. B. Han, Z. M. Zhang, T. Zheng, Y. G. Li, W. B. Lin, W. S.You, Z. M. Su and E. B. Wang, *J. Am. Chem. Soc.*, 2014, **136**,5359; (b) H. Fu, C. Qin, Y. Lu, Z. M. Zhang,Y. G. Li, Z. M. Su, W. L. Li and E. B. Wang, *Angew. Chem. Int. Ed.*, 2012, **51**, 7985; (c) S. T. Zheng, J. Zhang, X. X. Li, W. H. Fang and G. Y. Yang, *J. Am. Chem. Soc.*, 2010, **132**, 15102.

2 (a) Y. Q. Lan, S. L. Li, X. L. Wang, K. Z. Shao, D. Y. Du, H. Y. Zang and Z. M. Su, *Inorg. Chem.*, 2008, **47**, 8179; (b) M. Mirzaeia, H. Eshtiagh-Hosseini, M. Alipour and A. Frontera *Coord. Chem. Rev.*, 2014, **275**, 1; (c) X. K. Fang, P. Kogerler, L. Isaacs, S. Uchida and N. Mizuno, *J. Am. Chem. Soc.*, 2009, **131**, 432.

3 (a) X. L.Wang, Y. Q. Guo, Y. G. Li, E. B. Wang, C. W. Hu and N. H. Hu, *Inorg. Chem.*, 2003, **42**, 4135;(b) Q. G. Zhai, X. Y. Wu, S. M. Chen, Z. G. Zhao and C. Z. Lu, *Inorg. Chem.*, 2007, **46**, 5046;(c) Y. Y. Niu, L. F. Wang, X. R. Lv, H. J. Du, Y. Z. Qiao, H. W. Wang, L. S. Song, B. L. Wu, H. W. Hou and S. K. Weng, *CrystEngComm*, 2011, **13**, 5071.

4 (a) A. Iturrospe, L. S. Felices, S. Reinoso, B. Artetxe, L. Lezama and J. M. Gutié rrez-Zorrilla, *Cryst. Growth Des.*, 2014, **14**, 2318; (b) W. W. He, S. L. Li, H. Y. Zang, G. S. Yang, S. R. Zhang, Z. M. Su and Y. Q. Lan, *Coord. Chem. Rev.*, 2014, **279**, 141.

5 (a) C. J. Zhang, H. J. Pang, Q. Tang, H. Y. Wang and Y. G. Chen,, *Dalton Trans.*, 2010,**39**, 7993; (b) X. L. Wang, H. L. Hu and A. X. Tian, *Cryst. Growth Des.*, 2010,**10**, 4786; (c) B. K. Tripuramallu and S. K. Das, *Cryst. Growth Des.,* 2013, **13**, 2426; (d) J. Q. Sha, J. W. Sun, C. Wang, G. M. Li, P. F. Yan, M. T. Li and M. Y. Liu, *CrystEngComm.,* 2012, **14**, 5053.

6 (a) D. H. Yang, Y. F. Liang, P. T. Ma, S. Z. Li, J. P. Wang and J. Y. Niu, *CrystEngComm*, 2014,**16**, 8041; (b) F. J. Ma, S. X. Liu,. C. Y. Sun, D. D. Liang, G. J. Ren, F. Wei, Y. G. Chen, and Z. M. Su *J. Am. Chem. Soc.*, 2011, **133**, 4178; (c) X. L. Wang, Z. H. Chang, H. Y. Lin, A. X. Tian, G. C. Liu, J. W. Zhang and D. N. Liu, *RSC Adv.*, 2015, **5**, 14020.

7 (a) X. L. Wang, Z. H. Chang, H. Y. Lin, C. Xu, J. Luan, G. C. Liu and A. X. Tian, *RSC Adv.*, 2015, **5**, 35535; (b) X. L. Wang, C. Xu, H. Y. Lin, G. C. Liu, J. Luan and Z. H. Chang, *RSC Advances*, 2013, **3**, 3592; (c) X. L. Wang, C. Xu, H. Y. Lin, G. C. Liu, S. Yang, Q. Gao and A. X. Tian, *CrystEngComm*, 2012, **14**, 5836; (d) X. L. Wang, N. Xu, X. Z. Zhao, J. W. Zhang, C. H. Gong and T. J. Li, *CrystEngComm*, 2015, **17**, 7038; (e) H. Chen, H. An, X. Liu, H. Wang, Z.Chen, H. Zhang, Y. Hu, *Inorganica Chimica Acta.,* 2012, **21**, 65.

8 X. L. Wang, D. N. Liu, H. Y. Lin, G. C. Liu, X. Wang, M. Le and X. Rong, *CrystEngComm*, 2016, **18**, 888.

9 X. M. Chen, M.L. Tong, *Acc. Chem. Res.*, 2007, **40**, 162.

10 X. L. Wang, J. J. Cao, H. Y. Lin, G. C. Liu, J. Luan, A. X. Tian and J. W. Zhang, *Chin. Chem. Lett.*, 2013, **24**, 877.

11 (a) J. S. Goldsworthy, A. L. Pochodylo and R. L. LaDuca, *Inorg. Chim. Acta*, 2014, **419**, 26; (b) M. S. Chena, Z. S. Bai, Z. Su, S. S. Chen and W. Y. Sun, *Inorg. Chem. Commun.*, 2009, **12**, 530.

12 G. M. Sheldrick, Acta Crystallogr., Sect. A: Found. *Crystallogr.*, 2008, **64**, 112

13 A. L. Spek, Acta Crystallogr., Sect. D: Biol. *Crystallogr.*, 2009, **65**, 148.

14 (a) Y. Q. Lan, S. L. Li, Y. G. Li, Z. M. Su, K. Z. Shao and X. L. Wang, *CrystEngComm.*, 2008, **10**, 1129; (b) L. F. Ma, Y. Y. Wang,

L. Y. Wang, D. H. Lu, S. R. Batten and J. G. Wang, *Cryst. Growth Des.,* 2009, **9**, 2036.
15 (a) J. Rotzler, D. Vonlanthen, A. Barsella, A. Boeglin, A. Fort and M. Mayor, *Eur. J. Org. Chem.,* 2010, **6**, 1096; (b) X. L. Zhang, K. Luo, W. Chen and L. Wang, *Chin. J. Chem.*, 2011, **29**, 2209.
16 Y. Q. Lan, S. L. Li, X. L. Wang, K. Z. Shao, D. Y. Du, H. Y. Zang and Z M. Su, *Inorg. Chem.*, 2008, **47**, 8179.
17 H. Y. Liu, H. Wu, J. Yang, Y. Y. Liu, J. F. Ma and H. Y. Bai, *Cryst. Growth Des.*, 2011, **11**, 1786.
18 H. X. Yang, S. Y. Gao, J. Lü, B. Xu, J. X. Lin and R. Cao, *Inorg. Chem.*, 2010, **49**, 736.
19 B. Dolensky´, R. Konvalinka, M. Jakubek, V. Král, *J. Mol. Struct.*, 2013, **1035**, 124
20 K. Uehara, T. Oishi, T. Hirose and N. Mizuno, *Inorg. Chem.*, 2013, **52**, 11200.
21 (a) X. L. Wang, E. B. Wang, Y. Lan and C. W. Hu, *Electroanalysis*, 2002, **14**, 1116; (b) X. D. Du, C. H. Li, Y. Zhang, S. Liu, Y. Ma and X. Z. You, *CrystEngComm*, 2011, **13**, 2350.
22 (a) X. L. Wang, C. Xu, H. Y. Lin, G. C. Liu, J. Luan and Z. H. Chang, *RSC Adv.,*2013, **3** 3592; (b) A. X. Tian, Y. L. Ning, J. Ying, X. Hou, T. J. Li and X. L. Wang, *Dalton Trans.,*2015, **44**, 386.
23 M. L. Qi, K. Yu, Z. H. Su, C. X. Wang, C. M. Wang, B. B. Zhou and C. C. Zhu, *Dalton Trans.*, 2013, **42**, 7586.
24 (a) T. H. Li, Q. G. Li, J. Yan and F. Li, *Dalton Trans.*, 2014; **43**, 9061; (b) X. L. Wang, Z. H. Chang, H. Y. Lin, A. X. Tian, G. C. Liu and J. W. Zhang, *Dalton Trans.*, 2014, **43**, 12272.
25 (a) J. Rocha, L. D. Carlos, F. A. A. Paz, D. Ananias, *Chem. Soc. Rev.*, 2011, **40**, 926; (b) S. V. Eliseeva, J. C. G. Bunzli, *Chem. Soc. Rev.*, 2010, **39**, 189. (c) K. Binnemans, *Chem. Rev.*, 2009, **109**, 4283. (d) L. D. Carlos, R. A. S. Ferreira, V. de Zea Bermudez, P. Escribano, *Chem. Soc. Rev.*, 2011, **40**, 536. (e) S. H. Hwang, C. N. Moorefield, G. R. Newkome, *Chem. Soc. Rev.*, 2008, **37**, 2543.
26 (a) L. P. Zhang, J. F. Ma, J. Yang, Y. Y. Liu, G. H. Wei, *Cryst. Growth Des.*, 2009, **9**, 4660; (b) W. Q. Kan, J. Yang, Y. Y. Liu, J. F. Ma, *Inorg. Chem.*, 2012, **51**, 11266; (c) Z. Zheng, J. F. Ma, Y. Y. Liu, W. Q. Kan, J. Yang, *Cryst. Growth Des.*, 2013, **13**, 4338.